Journal of Translational Medicine

RESEARCH

Open Access

Radiation-sensitive circRNA hsa_circ_0096498 inhibits radiation-induced liver fibrosis by suppressing EIF4A3 nuclear translocation to decrease CDC42 expression in hepatic stellate cells

Peitao Zhou[1,2], Yixun Deng[3], Yining Sun[1,2], Dehua Wu[1,2*] and Yuhan Chen[1,2*]

Abstract

Background Radiation-induced liver fibrosis (RILF) is a common manifestation of radiation-induced liver injury (RILI) and is caused primarily by activated hepatic stellate cells (HSCs). Circular RNAs (circRNAs) play critical roles in various diseases, but little is known about the function and mechanism of circRNAs in RILF.

Methods RNA pull-down and liquid chromatography-tandem mass spectrometry (LC-MS/MS) were used to screen binding proteins of hsa_circ_0096498 (circ96498). RNA-binding protein immunoprecipitation, RNA pull-down and nuclear and cytoplasmic protein extraction were conducted to confirm the interaction between circ96498 and eukaryotic initiation factor 4A3 (EIF4A3). RNA sequencing was performed to screen target genes regulated by EIF4A3. HSCs with altered circ96498 and cell division cycle 42 (CDC42) expression were used to assess irradiated HSC activation. Circ96498 inhibition and CDC42 blockade were evaluated in RILF mouse models.

Results In this study, we identified a radiation-sensitive circ96498, which was highly expressed in the irradiated HSCs of paracancerous tissues from RILI patients. Circ96498 inhibited the proliferation but promoted the apoptosis of irradiated HSCs, suppressed the secretion of proinflammatory cytokines IL-1β, IL-6 and TNF-α, and decreased the expression of profibrotic markers (α-SMA and collagen 1) in irradiated HSCs. Mechanistically, irradiation induced the transport of EIF4A3 into the nucleus, and nuclear EIF4A3 increased the stability of *CDC42* mRNA and increased CDC42 expression, thereby promoting HSC activation through the NF-κB and JNK/Smad2 pathways. However, the binding of circ96498 to EIF4A3 impeded the translocation of EIF4A3 into the nucleus, resulting in the inhibition of CDC42 expression and subsequent HSC activation. Furthermore, circ96498 knockdown promoted the development of the early and late stages of RILF in a mouse model, which was mitigated by CDC42 blockade.

*Correspondence:
Dehua Wu
18602062748@163.com
Yuhan Chen
cspnr1@126.com

Full list of author information is available at the end of the article

Conclusions Collectively, our findings elucidate the involvement of the circ96498/EIF4A3/CDC42 axis in inhibiting irradiated HSC activation, which offers a novel approach for RILF prevention and treatment.

Graphical Abstract

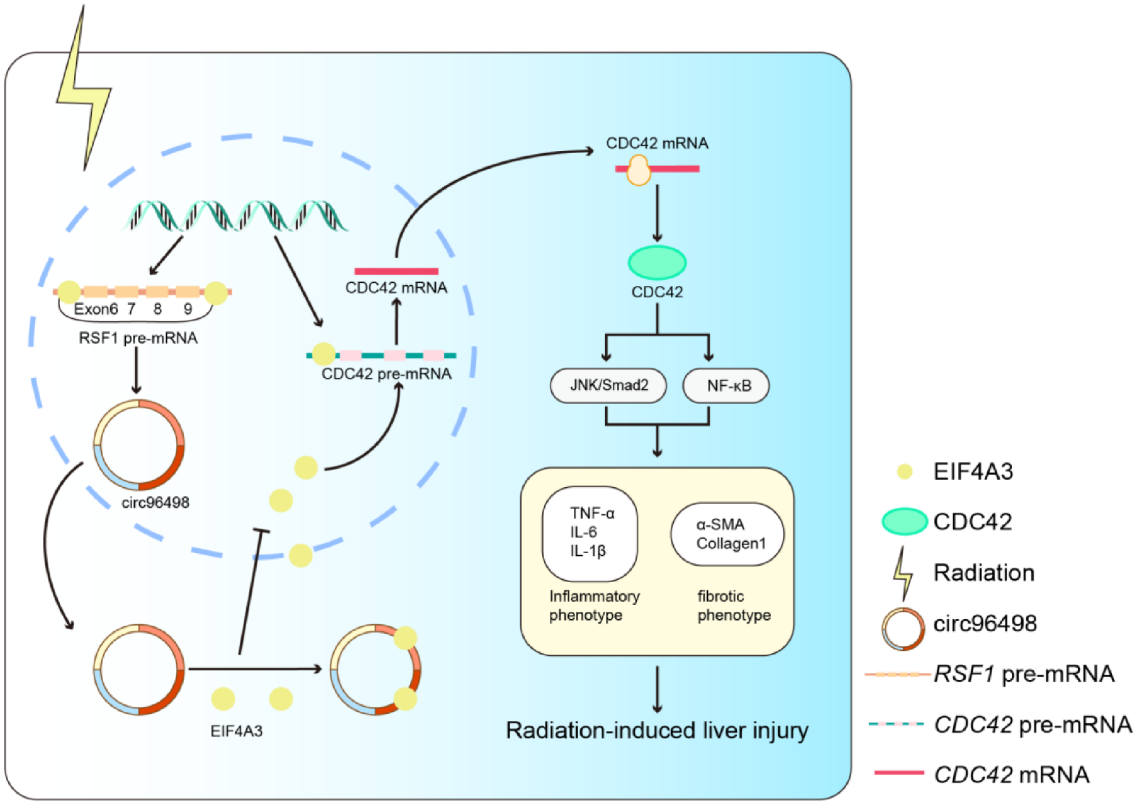

Keywords Circular RNA, EIF4A3, CDC42, Hepatic stellate cell, Radiation-induced liver fibrosis

Introduction

In recent years, with advances in radiotherapy technology and changes in dose segmentation mode, the effect of radiotherapy for multiple tumors, including primary hepatocellular carcinoma (HCC), has significantly improved [1, 2]. Currently, radiotherapy has become an important treatment for HCC [3]. However, 14.7% of HCC patients still suffer radiation-induced liver injury after stereotactic radiotherapy [4]. Radiation-induced liver injury is characterized mainly by hepatitis, liver fibrosis and even liver cirrhosis, leading to death in severe cases [5]. Thus, it is a type of radiation complication that cannot be ignored. Radiation-induced liver fibrosis (RILF) is the main manifestation of radiation-induced chronic liver injury. Hepatic stellate cells (HSCs) are key effector cells that mediate RILF. Radiation-induced HSC activation is a complex process involving a variety of cytokines and pathways [6, 7]. In our previous studies, we reported that radiation induces HSC activation through the NF-κB and JNK/Smad2 pathways, eventually promoting RILF development [8, 9]. A certain degree of liver fibrosis can be observed in the early stage of liver injury, indicating that HSC activation occurs in the initial stage of radiation injury [8, 10]. Therefore, inhibition of radiation-induced HSC activation is a potential strategy for the prevention and treatment of RILF.

Circular RNAs (circRNAs) are gene transcripts with covalently closed-loop structures and no polyadenylated tails [11]. CircRNAs are closely related to the occurrence and development of tumors, endocrine diseases, aging and other diseases [12]. CircRNAs exert various functions, such as participating in the regulation of parental gene expression, regulating the alternative splicing of transcripts, adsorbing microRNA (miRNA) as a miRNA sponge, directly binding to RNA-binding proteins (RBPs) or acting as scaffolds for RBPs, and even translating proteins [13]. We previously reported that the circRNA hsa_circ_0023706 transcribed from *RSF1* pre-mRNA was highly expressed in irradiated HSCs and increased RAC1 expression by sponging miR-146a-5p to promote

the inflammatory and fibrotic phenotype of HSCs [9]. Interestingly, we found that another circRNA hsa_circ_0096498 (circ96498) transcribed from *RSF1* pre-mRNA can inhibit radiation-induced inflammatory and fibrotic phenotypes of HSCs, suggesting that different circRNAs from the same transcript exert different regulatory effects. These findings prompted further exploration of the regulatory role of circ96498 in the pathogenesis of RILF to provide a new strategy for the prevention and treatment of RILF.

Materials and methods

Fluorescence in situ hybridization (FISH)

A Cy3-labeled circ96498 probe was designed and synthesized by RiboBio. A FISH kit (Cat. No. C10910, RiboBio) was used to detect the probe signals in liver tissues according to the manufacturer's instructions. In brief, the samples were fixed with 4% paraformaldehyde and pretreated with 0.5% Triton X-100. The circ96498 probe and human 18 S probe were subsequently used separately to hybridize with the samples at 37 °C, overnight. The cell nuclei were stained with 4,6-diamidino-2-phenylindole (DAPI, Beyotime, Shanghai, China). The images were scanned with a Pannoramic SCAN II (3DHISTECH, Hungary). The percentage of positive cells was analyzed using ImageJ software.

Isolation of hepatic stellate cells (HSCs)

Isolation of primary HSCs was performed as previously described [8, 14]. HSCs were isolated from the livers of the indicated C57BL/6 mice. Briefly, the livers of C57BL/6 mice were perfused through the portal vein with Hank's solution containing 0.05% collagenase IV (Cat. No. C8160, Solarbio Science & Technology, Beijing, China) and 0.01% DNase I (Cat. No. D8071, Solarbio Science & Technology, Beijing, China). After mechanical disruption, digestion for 15 min and filtration, the acquired cell suspension was centrifuged at 400 rpm for 5 min at 4 °C to remove the pellet containing primary hepatocytes. Non-parenchymal liver cells were collected by centrifuging the supernatants at 2000 rpm for 10 min at 4 °C. And HSCs were isolated through density gradient centrifugation. Isolated HSCs were cultured in DMEM (pH 7.4) supplemented with 10% (v/v) fetal bovine serum and a penicillin-streptomycin mixture (containing 100 μg/ml streptomycin sulfate and 100 U/ml penicillin G) (Cat. No. P1400, Solarbio Science & Technology, Beijing, China).

RNA pull-down

RNA pull-down was performed using a Pierce™ Magnetic RNA-Protein Pull-Down Kit (Cat. No. 20164, Thermo Fisher Scientific). The biotinylated DNA probe of circ96498 was incubated with streptavidin coated magnetic beads at 26 °C for 30 min to form probe-coated magnetic beads. LX2 cells transfected with si-circ96498 or control cells were cultured overnight with probe-coated beads at 4 °C. After washing, the bead-probe-circRNA mixture was eluted and extracted for western blot detection or mass spectrometry.

RNA-binding protein immunoprecipitation (RIP)

The transcripts that interacted with EIF4A3 were analyzed with a Magna RIP™ RNA-Binding Protein Immunoprecipitation Kit (Cat. No. 17-700, Millipore, Darmstadt, Germany). In brief, after the indicated treatments, the cells were collected and lysed in RIP lysis buffer. The magnetic beads were incubated with 5 μg anti-EIF4A3 antibody (Cat. No. 17504-1-AP, Proteintech, Rosemont, USA) or anti-mouse IgG (Millipore) with rotation for 30 min at room temperature. The supernatant from the cell lysate after centrifugation was added to each bead-antibody complex in RIP immunoprecipitation buffer with rotation for 3 h at 4 ℃. After the protein was digested with proteinase K buffer and washed carefully, the extracted RNA was purified and then analyzed by qRT-PCR. The percentage of input for each RIP sample was calculated as $\%\,\mathrm{input} = 2^{(\mathrm{Ct_{IP}}-(\mathrm{Ct_{input}}-\log_2[10]))}$.

Liquid chromatography-tandem mass spectrometry (LC-MS/MS)

The purified proteins from circ96498-overexpressing or control LX2 cells were separated by 10% SDS-PAGE and visualized by Coomassie blue staining. The bands of interest were subsequently excised, digested and lyophilized. The lyophilized peptide fractions were resuspended in ddH_2O containing 0.1% formic acid, and loaded into a nanoViper C18 (Acclaim PepMap 100, 75 μm×2 cm) trap column for liquid chromatography-tandem mass spectrometry (LC-MS/MS) analysis performed by Wininnovate Biotechnology (Shenzhen, China). The LC-MS/MS data were analyzed for protein identification and quantification using PEAKS Studio 8.5 (Bioinformatics Solutions Inc. Waterloo, Canada). The local false discovery rate at peptide spectrum matches was 1.0%. The precursor and fragment mass tolerances were set to 10 ppm and 0.05 Da, respectively.

In vivo animal studies

Female C57BL/6 mice (6–7 weeks old and 16–20 g) were maintained under pathogen-free conditions at the Experimental Animal Center of Southern Medical University. All animal experiments were specifically approved by the Southern Medical University Experimental Animal Ethics Committee (Approval Number: SMUL2022224, approval time: 10 November 2022). The mmu_circ_0013678 short hairpin RNA (shRNA) encapsulated by an adeno-associated virus containing the HSC-specific promoter of glial fibrillary acidic protein (HBAAV-*Gfap*-shcirc13678,

1×10^{12} vg/ml) was designed and synthesized by Hanbio Biotechnology (Shanghai, China). The mice were randomly grouped, and the right lobe of the liver was irradiated with X-rays (8 Gy×5 fractions, once a day), and a non-irradiated group served as a control. HBAAV-*Gfap*-shcirc13678 or vector (100 μl per mouse) was injected once via the tail vein one week before irradiation. The mice were treated with 10 mg/kg ML141 by intraperitoneal injection twice a week. The mice were sacrificed at 4 or 8 weeks after the last irradiation for evaluation of the early or late stage of RILF. At the end of the experiment, venous blood was drawn from the eye orbits of the mice, after which the mice were sacrificed. The serum levels of AST and ALT were detected via an automatic biochemistry analyzer. Portions of the liver tissues were collected for histological, immunohistochemistry and immunofluorescence analysis. The remaining fresh liver tissues were used for qRT-PCR analysis.

Patient samples

Twenty paracancerous samples were collected from HCC patients who received intrahepatic lesion radiotherapy from 2017 to 2021 (see Table S1 for patient details). The dose range of radiotherapy was 40 to 64.4 Gy with 6–30 fractions. All patients were examined by CT or MRI before and after radiotherapy. Each patient provided written informed consent. The study protocol was approved by the review committee of the Nanfang Hospital of Southern Medical University.

For imaging evaluation of radiation-induced liver injury, radiation-induced venous occlusive disease and liver fibrosis usually present as hypodensities on unenhanced CT. In contrast-enhanced CT, hypodensity can be observed in the arterial and portal venous phases, and hyperdensity or isodensity can even be observed in all enhanced phases. The irradiated area typically shows hypointensity and hyperintensity on T1-weighted images and T2-weighted images of MRI, respectively [15].

Results

Radiation-sensitive circ96498 inhibits irradiated HSC activation

To identify the expression and localization of circ96498 in human livers, we performed fluorescence in situ hybridization and found that circ96498 was significantly upregulated and located primarily in HSCs from patients with radiation-induced liver injury (RILI) (Fig. 1A). X-ray irradiation (8 Gy) significantly increased circ96498 expression in LX2 cells (Fig. 1B). Agarose gel electrophoresis revealed that the amplified products of the divergent primers for circ96498 could be detected in cDNA but not in gDNA (Fig. 1C). Circ96498 is formed by cyclization of exons 6–9 of the *RSF1* transcript. The junction site formed by the combination of exon 6 and exon 9 was also confirmed by Sanger sequencing (Fig. 1D). These results indicated that circ96498 is a covalently closed-loop RNA. After treatment with actinomycin D, *RSF1* mRNA expression was gradually decreased, but the change in circ96498 expression was not obvious (Fig. 1E). Similarly, *RSF1* mRNA expression was significantly downregulated after RNA enzyme treatment, but there was no significant change in the expression of circ96498 (Fig. 1F). The separation and detection of cell components indicated that circ96498 was expressed mainly in the cytoplasm (Fig. 1G). To explore the function of circ96498, a small interfering RNA (siRNA) and an overexpression plasmid for circ96498 were transfected into LX2 cells (Fig. 2A). Circ96498 inhibited proliferation but promoted apoptosis in irradiated LX2 cells (Fig. 2B, C and E). In addition, circ96498 suppressed the secretion of the proinflammatory cytokines IL-1β, IL-6 and TNF-α and decreased the expression of activation markers (α-SMA and collagen 1) in irradiated LX2 cells (Fig. 2D, F-I).

Circ96498 binds to EIF4A3 and inhibits EIF4A3 translocation into the nucleus to suppress irradiated HSC activation

To explore how circ96498 regulates HSC function, we performed an RNA pull-down assay in normal or circ96498-silenced irradiated LX2 cells and the extracted proteins were detected by liquid chromatography-tandem mass spectrometry (LC-MS/MS). The results revealed that the abundance of high mobility group box 1 (HMGB1) and eukaryotic translation initiation factor 4A3 (EIF4A3) in the circ96498 knockdown group decreased significantly (Fig. 3A-B). However, no obvious binding between circ96498 and HMGB1 was observed (Fig. 3C). But circ96498 could bind to EIF4A3, and circ96498 knockdown significantly reduced EIF4A3 binding (Fig. 3C). RIP detection also showed that EIF4A3 could bind to circ96498 (Fig. 3D). We subsequently predicted binding sites between circ96498 and EIF4A3 via *CircInteractome* (https://circinteractome.nia.nih.gov/) (Fig. 3E), and RIP detection confirmed that EIF4A3 could bind to predicted sites 1 (24–333) and 2 (1743–1978) (Fig. 3F). We further constructed a binding site 1 and site 2 deleted-circRNA overexpressing plasmid (circDel-OE) to transfect LX2 cells. RIP assay revealed that circ96498 overexpression promoted binding between EIF4A3 and circ96498, but circDel-OE transfection significantly decreased this interaction (Fig. 3G). In summary, circ96498 can bind to the EIF4A3 protein in HSCs.

To explore the role of EIF4A3 in irradiated HSC activation, we overexpressed or knocked down *EIF4A3* expression in LX2 cells (Figure S1A). We found that EIF4A3 promoted cell proliferation but inhibited cell apoptosis in irradiated LX2 cells (Figures S1B-C). And EIF4A3 increased the secretion of inflammatory factors (TNF-α,

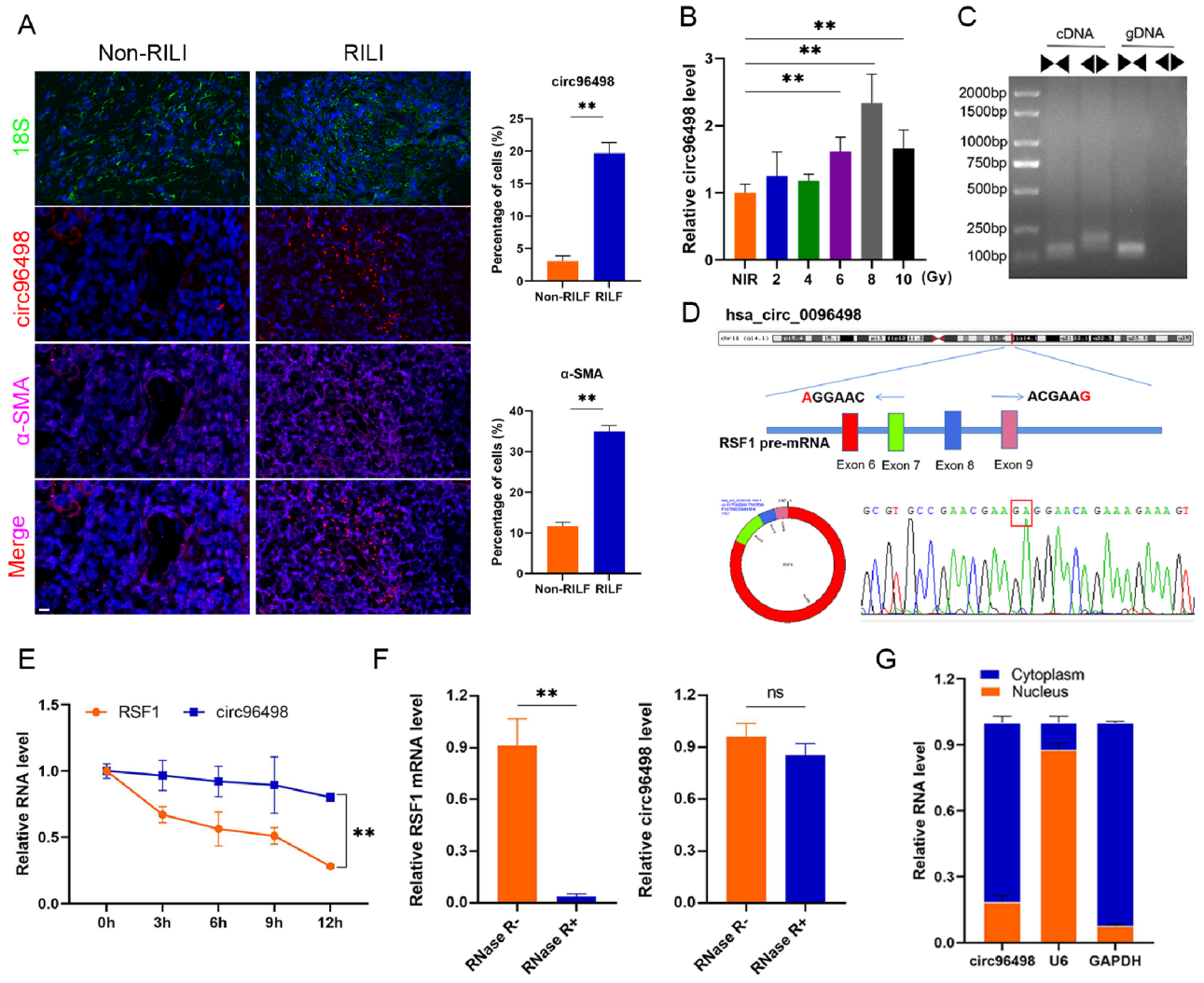

Fig. 1 Characterization of circ96498 in human HSCs. A. The location of circ96498 in human HSCs was detected with FISH and the percentage of circ96498- or α-SMA-positive cells was quantified ($n = 3$ per group). FISH, fluorescence in situ hybridization. Non-RILI, no radiation-induced radiation injury. RILI, radiation-induced radiation injury. B. The expression of circ96498 in LX2 cells treated with various doses of radiation was measured by qRT-PCR ($n = 3$ per group). C. Agarose gel electrophoresis revealed the products amplified by convergent or divergent primers for circ96498 in the complementary DNA (cDNA) and genomic DNA (gDNA) of LX2 cells. D. Schematic illustration of hsa_circ_0096498 formation. The back-splice junction sequences were validated by Sanger sequencing. E. The RNA expression levels of circ96498 and *RSF1* in LX2 cells were analyzed by qRT-PCR after treatment with actinomycin D for the indicated times ($n = 3$ per group). F. The abundances of circ96498 and linear *RSF1* mRNA in LX2 cells were detected after treatment with RNase R at the indicated time points ($n = 3$ per group). G. The RNA expression levels were determined by qRT-PCR after the nuclear and cytosolic separation of LX2 cells ($n = 3$ per group). GAPDH served as a cytoplasmic control and U6 was used as a nuclear control. Data are shown as mean ± SEM (**A**–**B** and **E**-**F**). Statistics are analyzed by unpaired Student's *t* test (two-tailed) (**A** and **F**), one-way ANOVA (**B**) and two-way ANOVA (**E**), followed by Tukey's test for multiple comparisons. $^{**}P < 0.01$, ns, no significance

IL-6 and IL-1β) and promoted the expression of profibrotic markers (α-SMA and collagen 1) in irradiated LX2 cells (Figures S1D-E). These results indicated that EIF4A3 promoted irradiated HSC activation, suggesting that circ96498 may modulate EIF4A3 expression to inhibit irradiated HSC activation. However, circ96498 did not affect EIF4A3 expression, and irradiation had no effect on EIF4A3 expression in LX2 cells (Figure S2A). Notably, EIF4A3 is a main component of the exon junction complex (EJC) [16], which binds the pre-mRNA to complete its splicing and transports mature mRNA from the nucleus to the cytoplasm to facilitate downstream processes, such as nonsense-mediated decay (NMD), mRNA localization and translation [17, 18]. Therefore, we hypothesized that irradiation and circ96498 may modulate EIF4A3 nuclear transport to regulate HSC activation. We found that irradiation and circ96498 knockdown promoted EIF4A3 translocation into the nucleus (Fig. 3H-I and S2B-C). These results suggest that circ96498

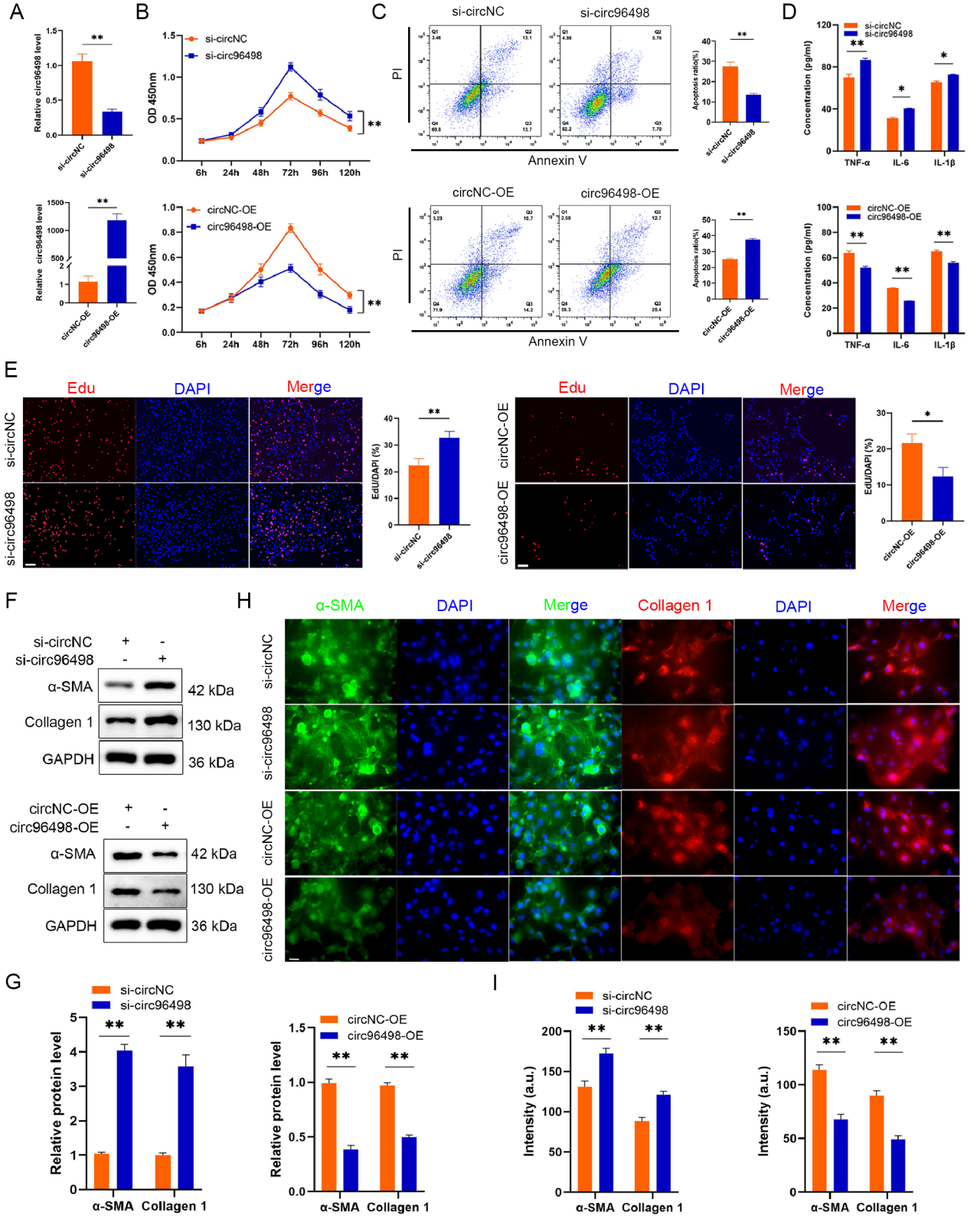

Fig. 2 (See legend on next page.)

(See figure on previous page.)

Fig. 2 Circ96498 inhibits irradiated HSC activation. A. RNA analysis of circ96498 in irradiated LX2 cells treated with circ96498 siRNA or the circ96498-overexpressing plasmid ($n=3$ per group). si-circ96498, circ96498 siRNA; si-circNC, negative control; circ96498-OE, circ96498-overexpressing plasmid; circNC-OE, circ96498-overexpressing negative control. B. CCK8 proliferation assay of irradiated LX2 cells transfected with si-circ96498 or circ96498-OE ($n=5$ per group). C. Apoptotic cell detection of irradiated LX2 cells transfected with si-circ96498 or circ96498-OE ($n=3$ per group). D. ELISA detection of TNF-α, IL-6 and IL-1β secreted by irradiated LX2 cells transfected with si-circ96498 or circ96498-OE ($n=3$ per group). E. EdU cell proliferation staining of irradiated LX2 cells transfected with si-circ96498 or circ96498-OE ($n=3$ per group). Scale bar, 50 μm. **F**-**G**. Western blot analysis of α-SMA and collagen 1 in irradiated LX2 cells transfected with si-circ96498 or circ96498-OE ($n=3$ per group). **H**-**I**. Immunofluorescence staining and quantification of α-SMA and collagen 1 in irradiated LX2 cells transfected with si-circ96498 or circ96498-OE ($n=3$ per group). Scale bar, 20 μm; a.u., arbitrary unit. Data are shown as mean ± SEM (**A**–**E**, **G** and **I**). Statistics are analyzed by unpaired Student's *t* test (two-tailed) (**A**, **C**-**E**, **G** and **I**) and two-way ANOVA (**B**). $^{*}P<0.05$, $^{**}P<0.01$

inhibits irradiation-induced EIF4A3 translocation into the nucleus in HSCs.

To identify whether circ96498 inhibits irradiated HSC activation in an EIF4A3-binding manner, we used importazole, a small molecule inhibitor of the nuclear transport receptor importin-β [19], to suppress EIF4A3 translocation into the nucleus. We confirmed that importazole efficiently inhibited EIF4A3 translocation into the nucleus (Figures S3A-C). Notably, treatment with importazole decreased proliferation and increased apoptosis and resulted in a decrease in proinflammatory and profibrotic factors in irradiated LX2 cells transfected with EIF4A3-OE (Figures S4A-F). To further investigate the impact of EIF4A3 nuclear translocation, we constructed a plasmid encoding EIF4A3-dNLS (EIF4A3 lacking the nuclear localization signal) as a dominant negative form. EIF4A3-dNLS evidently suppressed the translocation of EIF4A3 into the nucleus in irradiated LX2 cells (Figures S4G). Compared with EIF4A3-OE, EIF4A3-dNLS decreased the expression of proinflammatory and profibrotic factors in irradiated LX2 cells (Figures S4H-I). Notably, treatment with importazole showed decreased proliferation, increased apoptosis and resulted in a decrease in proinflammatory and profibrotic factors in irradiated LX2 cells transfected with si-circ96498 (Fig. 3J-M). Similarly, compared with circ96498-OE, circDel-OE, a plasmid lacking EIF4A3 binding sites, presented increased EIF4A3 translocation into the nucleus, increased proliferation and decreased apoptosis and increased levels of proinflammatory and profibrotic factors in irradiated LX2 cells (Fig. 3J-M and S3D). Interestingly, *CircInteractome* prediction found that EIF4A3 protein binding sites also exist in the transcript flanks of circ96498 (Figure S5A). RIP assay confirmed that EIF4A3 could bind to the flanking region of the circ96498 transcript (Figure S5B). Knocking down or overexpressing EIF4A3 inhibited or promoted the expression of circ96498, respectively (Figure S5C), suggesting that EIF4A3 promotes circ96498 expression. Collectively, circ96498 may inhibit EIF4A3 translocation into the nucleus to suppress irradiated HSC activation.

CDC42 promotes irradiated HSC activation

To clarify the mechanism by which EIF4A3 promotes irradiated HSC activation, we performed high-throughput sequencing of control and EIF4A3-silenced irradiated LX2 cells. Notably, 188 genes were differentially expressed in the si-EIF4A3 group and were enriched in pathways such as non-alcoholic fatty liver disease (Fig. 4A). Interestingly, the inflammatory and fibrotic phenotypes of HSCs are also essential events in the pathogenesis of non-alcoholic fatty liver disease [20], so we focused on genes enriched in non-alcoholic liver disease. Among them, cell division cycle 42 (*CDC42*), which is instrumental in cytoskeletal and microtubule dynamics, cell proliferation, cell cycle progression and apoptosis, has attracted our attention [21]. KEGG database showed that CDC42 is enriched in the MAPK pathway and modulates JNK phosphorylation (data not shown). We previously reported that irradiation induces the activation of the JNK/Smad2 pathway, which promotes HSC activation [8, 14]. Moreover, CDC42 showed an increase in the paracancerous tissues of patients with RILI, suggesting that CDC42 may predict the occurrence of RILI (Fig. 4B-C).

We further explored the role of CDC42 in HSC activation. In the RILF mouse model, CDC42 and α-SMA were colocalized in HSCs (Fig. 4D). Similarly, the colocalization of CDC42 and α-SMA in HSCs was also observed in patients with radiation-induced liver injury (Fig. 4E). Notably, irradiation increased CDC42 expression in LX2 cells (Fig. 4F). Furthermore, we found that CDC42 knockdown suppressed cell proliferation, promoted cell apoptosis and inhibited proinflammatory and profibrotic phenotypes in irradiated LX2 cells (Fig. 4G-K). Similarly, treatment with ML141, a potent and selective inhibitor of CDC42, led to the same results (Fig. 4G-K). Moreover, CDC42 knockdown or ML141 treatment inhibited the activation of the NF-κB and JNK/Smad2 pathways and reduced the expression of Bcl-2 and profibrotic markers (Fig. 4L-M). Together, these findings indicate that irradiation-induced CDC42 promotes irradiated HSC activation.

Circ96498 regulates CDC42 expression by binding to EIF4A3

To investigate whether circ96498 could mediate CDC42 expression through EIF4A3, we performed a RIP assay and found that EIF4A3 could bind to *CDC42* mRNA and that circ96498 knockdown promoted EIF4A3 and *CDC42*

A

Gene Symbol	-10lgP	FC(si-circNC/si-circ96498)
HMGB1	41.79	22.19
EIF4A3	146.95	14.55
DNJC9	89.49	13.24
RS14	53.17	12.37
NOP2	62.02	5.98
BCLF1	68.47	5.20
RBM14	88.45	4.68
MIC60	97.96	4.57
DX39B	76.32	4.40
PHB	111.89	4.04
MCCB	105.1	3.92
COX2	51.04	3.89
UCRI	51.66	3.59
PTBP1	123.26	3.57
HNRPM	211.69	3.38
DHX15	36.05	3.34
SCMC1	94.3	3.24
PDS5B	46.97	3.23
RSF1	94.06	3.10
TXTP	35.42	3.04

Fig. 3 (See legend on next page.)

(See figure on previous page.)

Fig. 3 Circ96498 binds to EIF4A3 and inhibits EIF4A3 translocation into the nucleus to suppress HSC activation. **A**. List of the main circ96498-binding RBPs identified by RNA pull-down and mass spectrometry (MS) analysis in irradiated LX2 cells. **B**. Best unique peptide-spectrum matches (PSMs) of HMGB1 and EIF4A3 by MS analysis. **C**. RNA pull-down assay to verify the interaction between circ96498 and HMGB1 or EIF4A3 using biotinylated probes targeting the circ96498 backspliced sequence. **D**. RNA-binding protein immunoprecipitation (RIP) assay analysis of the interaction between circ96498 and EIF4A3 ($n=3$ per group). **E**. Two putative EIF4A3 binding sites within the full-length circ96498 sequence. **F**. RIP assay analysis of the two binding sites between circ96498 and EIF4A3 ($n=3$ per group). **G**. RIP assay analysis of the binding between circ96498-OE or circDel-OE and EIF4A3. circDel-OE, the site 1 and site 2 deleted-circRNA overexpressing plasmid ($n=3$ per group). **H**. Western blot analysis of EIF4A3 expression in the cytoplasm or nucleus in irradiated LX2 cells transfected with si-circ96498 ($n=3$ per group). **I**. Immunofluorescence staining of EIF4A3 in irradiated LX2 cells transfected with si-circ96498. Scale bar, 20 μm. **J**-**L**. CCK8 proliferation assay (**J**), cell apoptosis detection (**K**) and ELISA detection of the concentrations of TNF-α, IL-6 and IL-1β (**L**) in irradiated LX2 cells with altered circ96498 expression and treated with either DMSO or the importin-β inhibitor importazole (5 μM) ($n=3$ per group). **M**. Immunofluorescence staining and quantification of α-SMA and collagen 1 in irradiated LX2 cells with altered circ96498 expression and treated with either DMSO or the importin-β inhibitor importazole (5 μM) ($n=3$ per group). Scale bar, 20 μm; a.u., arbitrary unit. Data are shown as mean ± SEM (**D**, **F**-**H** and **J**-**M**). Statistics are analyzed by unpaired Student's *t* test (two-tailed) (**F**), one-way ANOVA (**G** and **K**-**M**) and two-way ANOVA (**D**, **H** and **J**), followed by Tukey's test for multiple comparisons. $^{*}P<0.05$, $^{**}P<0.01$

mRNA binding (Fig. 5A). RNA stability assays revealed that EIF4A3 knockdown decreased *CDC42* mRNA stability (Fig. 5B). Notably, circ96498 decreased *CDC42* mRNA stability, whereas circDel-OE increased *CDC42* mRNA stability, indicating that circ96498 binds to EIF4A3 to decrease *CDC42* mRNA stability (Fig. 5C). In the RILF mouse model and patients with RILI, EIF4A3 and CDC42 were enriched in HSCs, and the abundance of EIF4A3 in the nucleus increased (Fig. 5D-E). Compared with si-circ96498, importazole substantially decreased CDC42 expression and suppressed the activation of the NF-κB and JNK/Smad2 pathways in irradiated LX2 cells (Fig. 5F). Additionally, compared with the circ96498-OE group, circDel-OE efficiently increased CDC42 expression and promoted the activation of the NF-κB and JNK/Smad2 pathways in irradiated LX2 cells, whereas circDel-OE resulted in an increase in CDC42 expression (Fig. 5G). Together, these findings indicate that circ96498 binds to EIF4A3 to inhibit EIF4A3 translocation into the nucleus to decrease *CDC42* mRNA stability, resulting in decreased CDC42 expression and suppressed activation of the NF-κB and JNK/Smad2 pathways.

Circ96498 inhibits irradiated HSC activation by modulating CDC42

Next, we explored whether circ96498 inhibits irradiated HSC activation in a CDC42-dependent manner. Notably, compared with circ96498 knockdown, combined circ96498 and CDC42 knockdown significantly inhibited cell proliferation, increased cell apoptosis, decreased TNF-α, IL-6 and IL-1β secretion, suppressed α-SMA and collagen 1 expression and inhibited the activation of the NF-κB and JNK/Smad2 pathways in irradiated LX2 cells (Fig. 6A-G). Moreover, CDC42 overexpression significantly attenuated the effects of circ96498 overexpression on cell proliferation, apoptosis, the expression of proinflammatory and profibrotic factors and the activation of the NF-κB and JNK/Smad2 pathways (Fig. 6A-G). Collectively, these results demonstrate that circ96498 suppresses irradiated HSC activation in a CDC42-dependent manner.

CDC42 inhibition alleviates the effect of circ13678 knockdown on the RILF mouse model

To further confirm the role of circ96498 in RILF in vivo, we identified the corresponding conserved circRNA of circ96498 in mice, named mmu_circ_0013678 (circ13678), according to the CircBank database (http://www.circbank.cn/). Similarly, irradiation upregulated circ13678 expression in mouse HSCs (Figure S6A). And circ13678 knockdown decreased cell apoptosis, promoted TNF-α, IL-6 and IL-1β secretion, and increased profibrotic factor expression in irradiated mouse HSCs (Figure S6B-E). Notably, circ13678 knockdown had no significant effect on EIF4A3 expression, but promoted CDC42 expression in irradiated mouse HSCs (Figure S6F). Furthermore, RIP confirmed that EIF4A3 could bind to circ13678, and circ13678 knockdown decreased the binding of circ13678 and EIF4A3 but increased the binding of CDC42 and EIF4A3 (Figure S6G).

Next, we explored the effects of circ13678 and CDC42 on the RILF mouse model. We constructed HBAAV-*Gfap*-shcirc13678 to specifically knockdown circ13678 in mouse HSCs and administered the CDC42 inhibitor ML141 (10 mg/kg) to irradiated mice. The mice were sacrificed at 4 weeks after the last irradiation for evaluation of the early stage of RILF (Fig. 7A). Significantly, HBAAV-*Gfap*-shcirc13678 decreased circ13678 expression in mouse HSCs (Fig. 7B). In addition, circ13678 knockdown increased the serum levels of AST and ALT (Fig. 7C). After circ13678 knockdown, α-SMA around vessels and perivascular collagen deposition significantly increased (Fig. 7D). Immunofluorescence showed that circ13678 knockdown increased EIF4A3 translocation into the nucleus, enhanced CDC42 expression, and obviously increased the coexpression of CDC42 and α-SMA in HSCs (Fig. 7E). Interestingly, the administration of ML141 significantly attenuated the effect of circ13678 knockdown (Fig. 7C-E). Together, the above results indicate that circ13678 knockdown in HSCs promotes RILF, which can be alleviated by CDC42 inhibition. In addition, circ13678 deficiency increased the expression of proinflammatory genes (*Il-1β*, *Il-6* and *Tnf-α*) in irradiated

liver tissues and increased the serum levels of IL-1β, IL-6 and TNF-α (Fig. 7F-G). Circ13678 knockdown substantially increased the infiltration of macrophages ($F4/80^+$ cells) into the liver (Fig. 7H-I). Notably, treatment with ML141 significantly alleviated these effects (Fig. 7F-I). Collectively, these results suggest that in irradiated mouse livers, circ13678 knockdown in HSCs promotes the release of proinflammatory cytokines and the infiltration of proinflammatory cells, and thus induces the formation of the hepatic inflammatory microenvironment, but CDC42 inhibition can efficiently alleviate the effect of circ13678 knockdown on the RILF mouse model.

Furthermore, we evaluated the effects of circ13678 knockdown and ML141 treatment on the late stage of RILF (Figure S7A). Similarly, circ13678 knockdown increased the serum levels of AST and ALT and the serum levels of IL-1β, IL-6 and TNF-α and increased α-SMA expression and collagen deposition in irradiated liver tissues, which was significantly attenuated by CDC42 inhibition (Figures S7B-D).

Discussion

CircRNAs bind to different RBPs to form specific complexes, which then affect the regulatory effect of RBPs [22]. In this study, protein spectrum detection and related experiments confirmed that circ96498 exerts its function through binding to EIF4A3. EIF4A3 plays an important role in the splicing, decay, nuclear export, subcellular localization and translation efficiency of mRNAs [23]. At present, there are three interaction modes between circRNAs and EIF4A3. First, EIF4A3 most commonly regulates circRNA generation by binding the flanking regions of circRNA transcripts. In most cases, EIF4A3 promotes circRNA generation [24–27]. In our study, irradiation promoted the transport of EIF4A3 into the nucleus, where it bound the flanking regions of the circ96498 transcript to promote circ98498 generation. However, a few studies have reported that EIF4A3 inhibits the formation of circRNAs. For example, EIF4A3 inhibits the expression of circ_100290 in gastric cancer and circ_0087429 in cervical cancer [25, 28]. Second, circRNAs recruit EIF4A3 to bind and increase the stability of target mRNAs. For example, circ_0055412 recruits EIF4A3 to stabilize *CAPG* mRNA and thus promotes glioma resistance to cisplatin [29]. CircETFA recruits EIF4A3 to prolong the half-life of *CCL5* mRNA to promote HCC development [30]. Hsa_circ_0068631 recruits EIF4A3 to increase the stability of *c-Myc* mRNA to promote breast cancer progression [28]. Moreover, circRNAs can reduce the binding of EIF4A3 and target mRNAs and downregulate the expression of target mRNAs. For example, hsa_circ_0030042 inhibits autophagy by sponging EIF4A3 and blocking EIF4A3 recruitment to *BECN1* and *FOXO1* mRNAs, resulting in the downregulation of BECN1 and FOXO1 [31]. Circ_0004296 inhibits the metastasis of prostate cancer by binding to EIF4A3 and inhibiting the nuclear export of *ETS1* mRNA mediated by EIF4A3, resulting in decreased ETS1 expression [32]. The current study revealed that circ96498 reduced EIF4A3 and CDC42 binding, leading to decreased stability and expression of CDC42, thereby inhibiting HSC activation induced by irradiation. On the basis of this evidence, we speculate that the interaction between circRNAs and the EIF4A3 protein may be related to different disease backgrounds. The expression level, cellular distribution and binding sites of circRNAs and EIF4A3, as well as the activation status of downstream target genes, may affect the interaction mode of circRNAs and EIF4A3. Therefore, under different conditions, circRNAs can act as "sponges" or protein scaffolds for EIF4A3, resulting in different functions of EIF4A3.

CDC42 is one of the most important members of the Rho-GTP family, and plays an important role in controlling gene transcription, regulating the cell cycle, cytoskeleton, cell movement and polarization [21]. In addition, CDC42 has been shown to promote the migration and activation of HSCs [33, 34]. However, the role and mechanism of CDC42 in regulating irradiated HSC activation are still unclear. CDC42 regulates multiple signaling pathways, such as the JNK and p38/MAPK pathways, to regulate gene transcription [35]. CDC42 can also activate p21-activated kinase 1 to promote the downstream TRAF6/NF-κB inflammatory signaling pathway [36]. Our current study revealed that CDC42 inhibition suppressed the NF-κB and JNK/Smad2 signaling pathways and repressed the irradiated HSC activation. The mouse model showed that CDC42 inhibitors could effectively alleviate RILF. Clinical data also confirmed that high expression of CDC42 in liver tissue was closely related to radiation-induced liver injury. These results indicate the potential value of inhibiting CDC42 in the prevention and treatment of RILF. At present, a variety of small molecule inhibitors of CDC42 have been developed, but most studies on these inhibitors have not been carried out in clinical practice [37]. The application of CDC42 inhibitors in the prevention and treatment of radiation-induced liver injury is worth considering in future clinical trials.

Given that circRNAs are usually expressed in a tissue- or cell type-specific manner and have structural stability in body fluids, they can be used as rapid and noninvasive biomarkers for early diagnosis and potential promising targets for disease treatment [38]. Circular RNA expression plasmids and RNA interference strategies are commonly used for gain-of-function and loss-of-function approaches, respectively. However, there are limitations to these strategies, including their lack of cell specificity, instability, off-target effects and immune

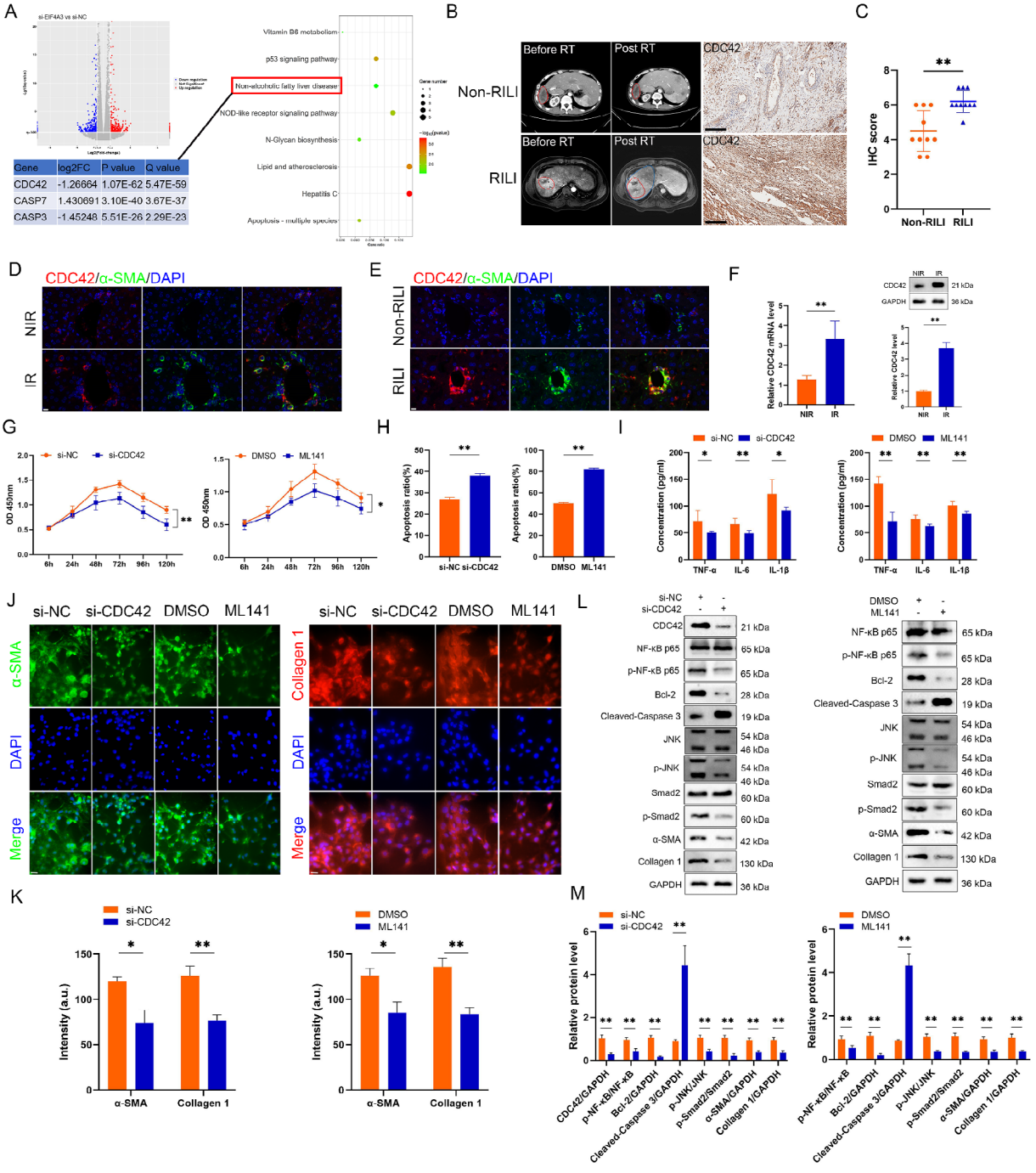

Fig. 4 CDC42 promotes irradiated HSC activation. **A**. Volcano plot and KEGG analysis of differentially expressed genes in irradiated LX2 cells treated with or without si-EIF4A3. Genes with FDR-corrected *P* values < 0.05 are highlighted. The dotted lines indicate 2-fold changes. **B**. Representative MRI images before and after radiotherapy (RT) from HCC patients with or without radiation-induced liver injury (RILI). The red lines indicate the tumor area and the blue lines indicate the RILI area. IHC staining of CDC42 in paracancerous liver tissue from corresponding patients who underwent surgical resection before radiotherapy. Scale bar, 200 μm. **C**. IHC score of CDC42 in paracancerous liver tissue from HCC patients with or without RILI ($n = 10$ per group). **D**-**E**. Multiplex immunofluorescence staining was conducted on liver tissues from C57BL/6 mice 4 weeks after irradiation or without irradiation (**D**) or from HCC patients with or without RILI (**E**). Scale bar, 10 μm. **F**. Western blot and mRNA analysis of CDC42 expression in LX2 cells with or without irradiation ($n = 3$ per group). **G**-**I**. CCK8 proliferation assay (G), cell apoptosis detection (H) and ELISA detection of the concentrations of TNF-α, IL-6 and IL-1β (I) in irradiated LX2 cells transfected with si-CDC42 or treated with ML141 (5 μM) ($n = 3$ per group). **J**-**K**. Immunofluorescence staining and quantification of α-SMA and collagen 1 in irradiated LX2 cells transfected with si-CDC42 or treated with ML141 (5 μM) for 48 h ($n = 3$ per group). Scale bar, 20 μm; a.u., arbitrary unit. **L**-**M**. Western blot analysis of related proteins in irradiated LX2 cells transfected with si-CDC42 or treated with ML141 (5 μM) for 48 h ($n = 3$ per group). Data are shown as mean ± SEM (**C**, **F**–**I**, **K** and **M**). Statistics are analyzed by nonparametric Mann-Whitney *U* test (**C**), unpaired Student's *t* test (two-tailed) (F, H-I, K and M) and two-way ANOVA (**G**). **P* < 0.05, ***P* < 0.01

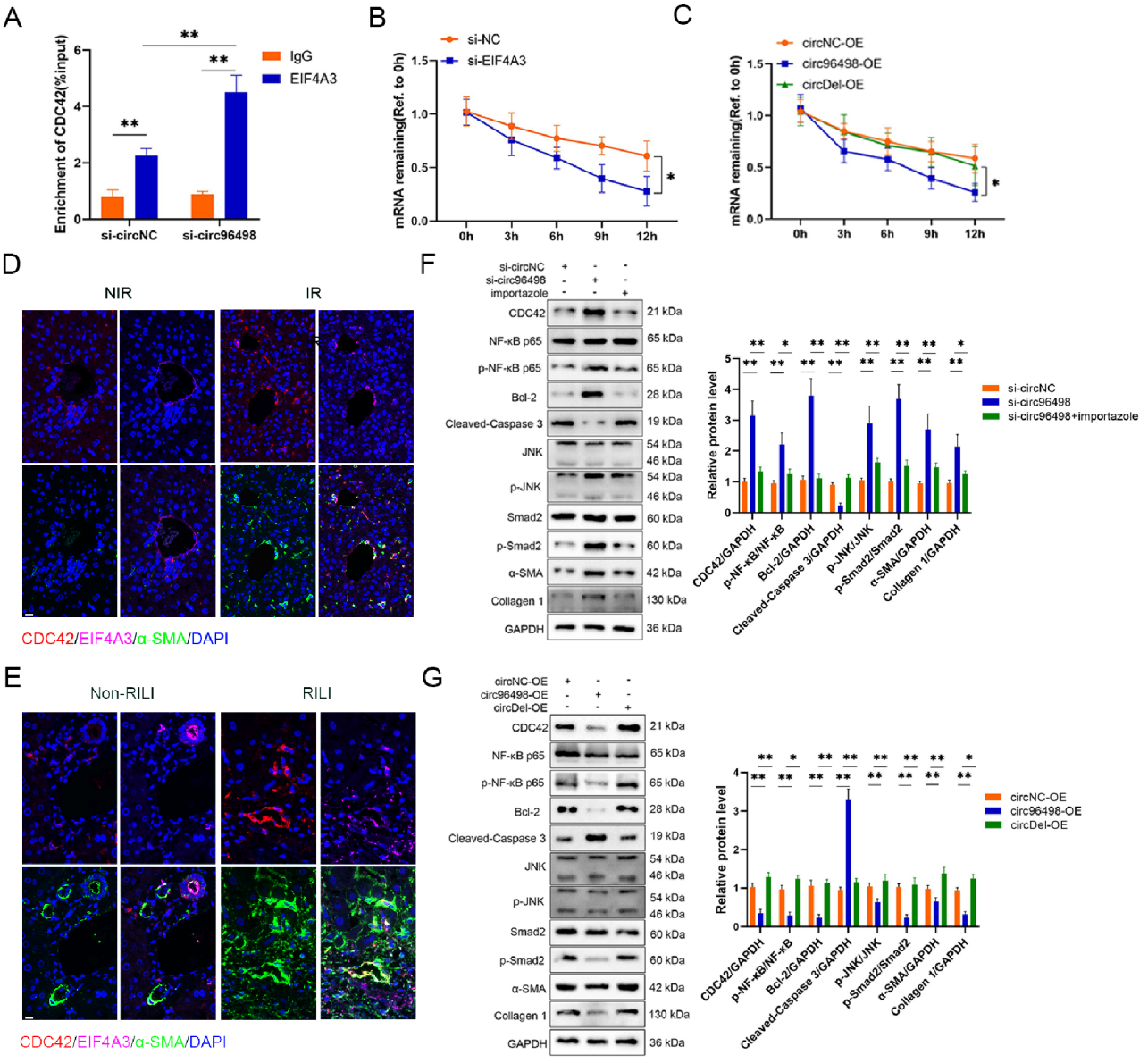

Fig. 5 Circ96498 regulates CDC42 expression by binding to EIF4A3. **A**. RIP assay analysis of the interaction between EIF4A3 and *CDC42* mRNA in irradiated LX2 cells ($n = 3$ per group). **B**. *CDC42* mRNA expression was analyzed after treatment with actinomycin D in irradiated LX2 cells transfected with si-EIF4A3 ($n = 3$ per group). **C**. *CDC42* mRNA expression was analyzed after treatment with actinomycin D in irradiated LX2 cells transfected with circ96498-OE or circDel-OE ($n = 3$ per group). **D**-**E**. Multiplex immunofluorescence staining was conducted on liver tissues from C57BL/6 mice (**D**) with or without irradiation or from HCC patients (**E**) with or without RILI. Scale bar, 10 μm. RILI, radiation-induced liver injury. **F**-**G**. Western blot analysis of related proteins in irradiated LX2 cells treated with si-circ96498 and the importin-β inhibitor importazole (5 μM) for 48 h (**F**) or with circ96498-OE or circDel-OE (G) ($n = 3$ per group). Data are shown as mean ± SEM (**A**-**C** and **F**-**G**). Statistics are analyzed by two-way ANOVA (**A**-**C**) and one-way ANOVA (**F**-**G**), followed by Tukey's test for multiple comparisons. $^{*}P < 0.05$, $^{**}P < 0.01$

activation [39, 40]. Employing nanoparticles or exosomes as delivery vectors for these molecules can increase their stability, facilitate their intracellular uptake, and modulate their immunogenicity [41]. For example, delivery of nanoparticle-conjugated circYap mitigated cardiac fibrosis and enhanced heart function in mice [42]. Furthermore, owing to the unique anatomical features of the liver, it serves as a primary site for the retention of

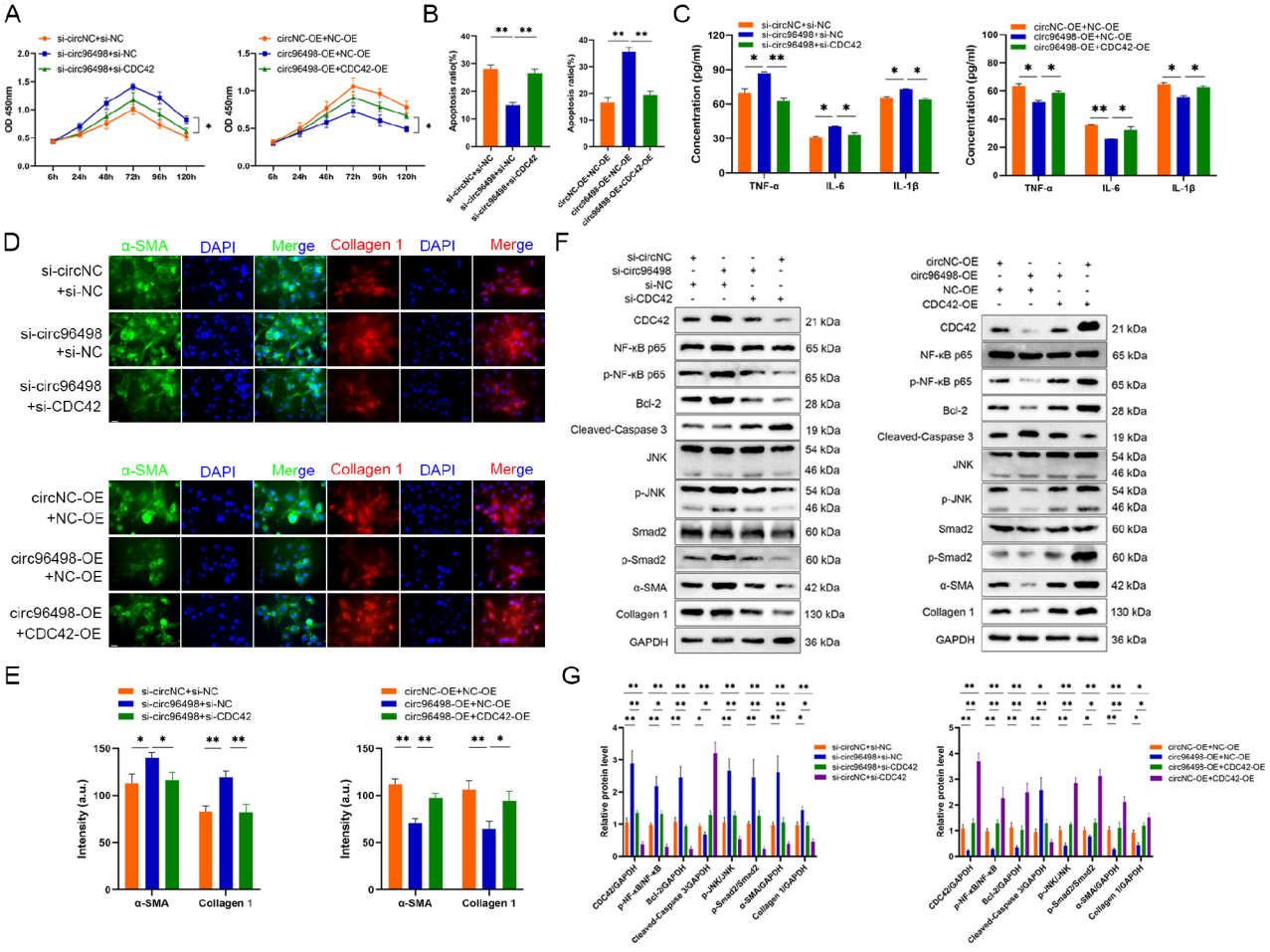

Fig. 6 Circ96498 inhibits irradiated HSC activation through modulating CDC42. **A-C**. CCK8 proliferation assay (**A**), cell apoptosis detection (**B**) and ELISA detection of the concentrations of TNF-α, IL-6 and IL-1β (**C**) in irradiated LX2 cells with altered circ96498 and CDC42 expression ($n = 3$ per group). **D**-**E**. Immunofluorescence staining and quantification of α-SMA and collagen 1 in irradiated LX2 cells with altered circ96498 and CDC42 expression ($n = 3$ per group). Scale bar, 20 μm; a.u., arbitrary unit. **F**-**G**. Western blot analysis of related proteins in irradiated LX2 cells with altered circ96498 and CDC42 expression ($n = 3$ per group). Data are shown as mean ± SEM (**A-C**, **E** and **G**). Statistics are analyzed by two-way ANOVA (**A**), one-way ANOVA (**B-C**, **E** and **G**), followed by Tukey's test for multiple comparisons. $^{*}P < 0.05$, $^{**}P < 0.01$

nanoparticles, especially larger particles [43]. After surface modification, nanoparticles can be selectively directed to the liver, thereby enhancing the delivery of therapeutic agents and minimizing adverse effects [44]. In our study, we confirmed that the radiation-sensitive circ96498 is predominantly expressed in HSCs and inhibits the activation of irradiated HSCs. These findings suggest that circ96498 could serve as a rapid and noninvasive biomarker for early diagnosis and a potential therapeutic target for RILF. Further investigation into the use of nanoparticle-conjugated circ96498 for RILF treatment is warranted, as it may represent a promising therapeutic approach.

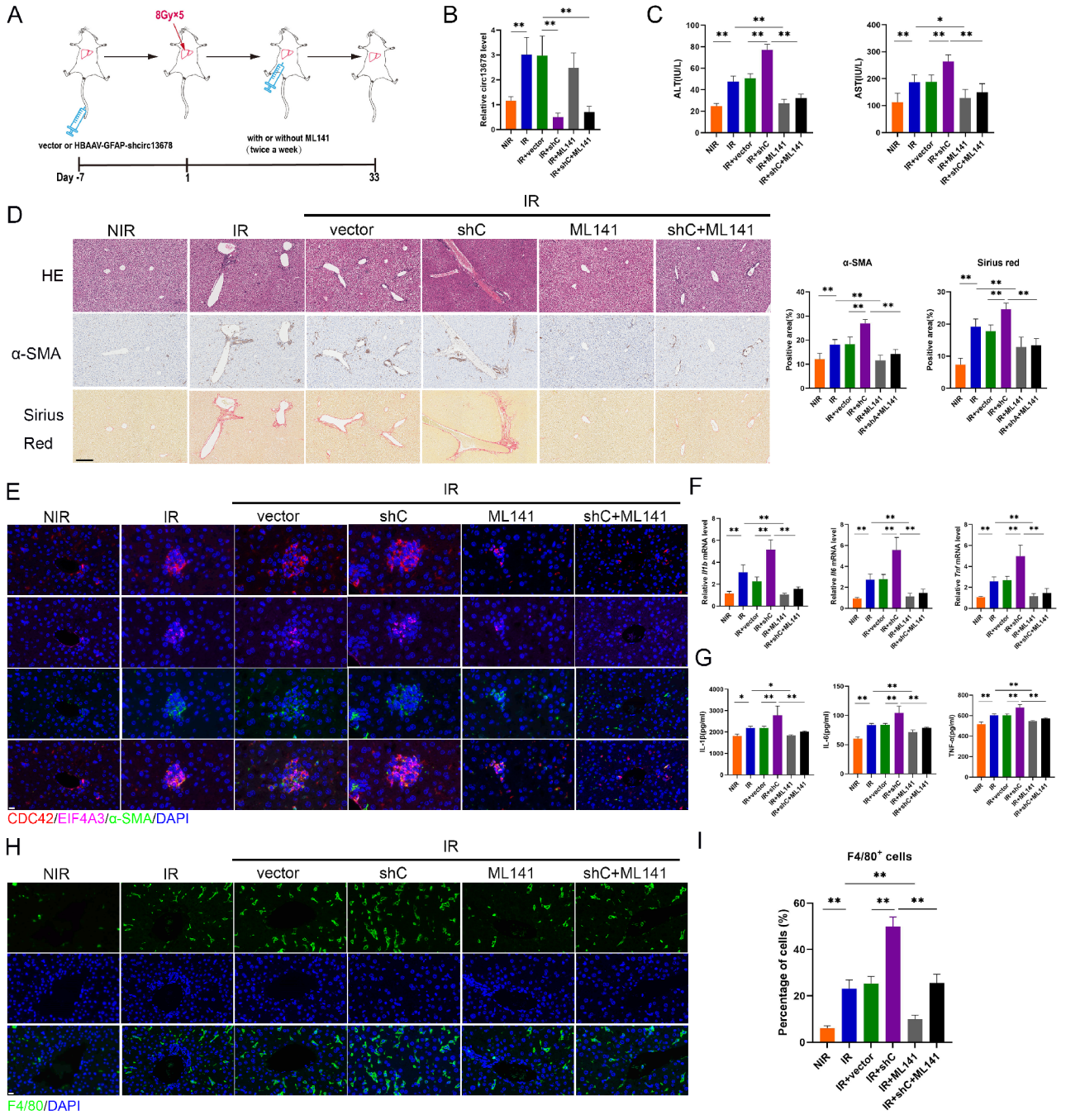

Fig. 7 CDC42 inhibition alleviates the promoting effect of circ13678 knockdown on the RILF mouse model. **A**. Schematic overview of the treatment of RILF mouse model. **B**. The circ13678 RNA level in HSC from indicated mice ($n=5$ per group). NIR, nonirradiation; IR, irradiation; shC, HBAAV-*Gfap*-shcirc13678; ML141, CDC42 inhibitor. **C**. The serum levels of ALT and AST in mice after the indicated treatments ($n=5$ per group) **D**. Hematoxylin eosin (HE), immunohistochemistry (IHC) staining of α-SMA and Sirius red staining in liver tissues from indicated mice ($n=5$ per group). Scale bar, 200 μm. **E**. Multiplex immunofluorescence staining in liver tissues from indicated mice. Scale bar, 10 μm. **F**. The mRNA levels of *Il1b*, *Il6* and *Tnf* in liver tissues from indicated mice ($n=5$ per group). **G**. ELISA detection of the concentration of IL-1β, IL-6 and TNF-α in serum from indicated mice ($n=5$ per group). **H-I**. Immunofluorescence staining and quantification of F4/80$^+$ cells in liver tissues from indicated mice ($n=5$ per group). Scale bar, 10 μm. Data are shown as mean ± SEM (**B-D**, **F-G** and **I**). Statistics are analyzed by one-way ANOVA (**B-D**, **F-G** and **I**), followed by Tukey's test for multiple comparisons. *$P<0.05$, **$P<0.01$

Conclusions

In conclusion, irradiation promotes EIF4A3 translocation into the nucleus, which induces high circ96498 levels in HSCs. Notably, circ96498 binds to the EIF4A3 protein to inhibit EIF4A3 translocation into the nucleus, resulting in unstable *CDC42* mRNA and thus a reduction in the CDC42 protein, which represses the activation of the NF-κB and JNK pathways to inhibit irradiated HSC activation, and thus suppresses radiation-induced liver fibrosis. This study elucidates the pathogenesis mechanism and provides new ideas for the prevention and treatment of RILF.

Supplementary Information

The online version contains supplementary material available at https://doi.org/10.1186/s12967-024-05695-6.

Supplementary Material 1

Acknowledgements
None.

Author contributions
YC, DW, and PZ conceived and designed the study. PZ and YD conducted experiments, analyzed the data and drafted the initial manuscript. PZ and YS prepared the figures for the manuscript. YC and PZ revised the initial manuscript. YC and DW supervised all the processes in this manuscript. All authors reviewed and approved the final manuscript.

Funding
This study was supported by National Natural Science Foundation of China (Grant No. 81903132, 82272737 and 82073394), Science and Technology Program of Guangzhou (Grant No. 202102020013), Basic and Applied Basic Research Foundation of Guangdong Province (Grant No. 2022B1515120035), National College Students' Innovation and Entrepreneurship Training Program (Grant No. 202112121011 and 202212121251) and Outstanding Youth Development Scheme of Nanfang Hospital, Southern Medical University (Grant No. 2019J006).

Data availability
The data that support the findings of this study are available in the supplementary material of this article or available from the corresponding author upon reasonable request.

Declarations

Ethics approval and consent to participate
The study was specifically approved by the Southern Medical University Experimental Animal Ethics Committee (Approval Number: SMUL2022224, approval time: 10 November 2022) and was conducted in accordance with the principles of the Helsinki Declaration. Written informed consent was obtained from all patients prior to enrollment.

Consent for publication
Not applicable.

Competing interests
The authors declare that they have no competing interests.

Author details
[1]Department of Radiation Oncology, Nanfang Hospital, Southern Medical University, Guangzhou, Guangdong Province 510515, China
[2]Guangdong Provincial Key Laboratory for Prevention and Control of Major Liver Diseases, Guangzhou, Guangdong Province 510515, China
[3]The First School of Clinical Medicine, Southern Medical University, Guangzhou, Guangdong Province 510515, China

Received: 11 April 2024 / Accepted: 20 September 2024
Published online: 01 October 2024

References

1. Wei X, Jiang Y, Zhang X, Feng S, Zhou B, Ye X, et al. Neoadjuvant three-Dimensional Conformal Radiotherapy for Resectable Hepatocellular Carcinoma with Portal Vein Tumor Thrombus: a randomized, Open-Label, Multicenter Controlled Study. J Clin Oncol. 2019;37(24):2141–51.
2. Montazersaheb S, Jafari S, Aytemir MD, Ahmadian E, Ardalan M, Zor M, et al. The synergistic effects of betanin and radiotherapy in a prostate cancer cell line: an in vitro study. Mol Biol Rep. 2023;50(11):9307–14.
3. Chen B, Wu J-X, Cheng S-H, Wang L-M, Rong W-Q, Wu F, et al. Phase 2 study of Adjuvant Radiotherapy following narrow-margin hepatectomy in patients with HCC. Hepatology. 2021;74(5):2595–604.
4. Long Y, Liang Y, Li S, Guo J, Wang Y, Luo Y, et al. Therapeutic outcome and related predictors of stereotactic body radiotherapy for small liver-confined HCC: a systematic review and meta-analysis of observational studies. Radiat Oncol. 2021;16(1):68.
5. Jia J, Sun J, Duan X, Li W. Clinical values and markers of Radiation-Induced Liver Disease for Hepatocellular Carcinoma with Portal Vein Tumor Thrombus treated with stereotactic body Radiotherapy. Front Oncol. 2021;11:760090.
6. Zhu W, Zhang X, Yu M, Lin B, Yu C. Radiation-induced liver injury and hepatocyte senescence. Cell Death Discov. 2021;7(1):244.
7. Ommati MM, Sabouri S, Sun Z, Zamiri MJ, Retana-Marquez S, Nategh Ahmadi H, et al. Inactivation of Mst/Nrf2/Keap1 signaling flexibly mitigates MAPK/NQO-HO1 activation in the reproductive axis of experimental fluorosis. Ecotoxicol Environ Saf. 2024;271:115947.
8. Chen Y, Wu Z, Yuan B, Dong Y, Zhang L, Zeng Z. MicroRNA-146a-5p attenuates irradiation-induced and LPS-induced hepatic stellate cell activation and hepatocyte apoptosis through inhibition of TLR4 pathway. Cell Death Dis. 2018;9(2):22.
9. Chen Y, Yuan B, Chen G, Zhang L, Zhuang Y, Niu H, et al. Circular RNA RSF1 promotes inflammatory and fibrotic phenotypes of irradiated hepatic stellate cell by modulating miR-146a-5p. J Cell Physiol. 2020;235(11):8270–82.
10. Wang S, Hyun J, Youn B, Jung Y. Hedgehog signaling regulates the repair response in mouse liver damaged by irradiation. Radiat Res. 2013;179(1):69–75.
11. Liu C-X, Chen L-L. Circular RNAs: characterization, cellular roles, and applications. Cell. 2022;185(12):2016–34.
12. Lei K, Bai H, Wei Z, Xie C, Wang J, Li J, et al. The mechanism and function of circular RNAs in human diseases. Exp Cell Res. 2018;368(2):147–58.
13. Yang L, Wilusz JE, Chen L-L. Biogenesis and Regulatory roles of Circular RNAs. Annu Rev Cell Dev Biol. 2022;38:263–89.
14. Tan J, Fan W, Liu T, Zhu B, Liu Y, Wang S, et al. TREM2(+) macrophages suppress CD8(+) T-cell infiltration after transarterial chemoembolisation in hepatocellular carcinoma. J Hepatol. 2023;79(1):126–40.
15. Takamatsu S, Kozaka K, Kobayashi S, Yoneda N, Yoshida K, Inoue D, et al. Pathology and images of radiation-induced hepatitis: a review article. Jpn J Radiol. 2018;36(4):241–56.
16. Andersen CBF, Ballut L, Johansen JS, Chamieh H, Nielsen KH, Oliveira CLP, et al. Structure of the exon junction core complex with a trapped DEAD-box ATPase bound to RNA. Science. 2006;313(5795):1968–72.
17. Andreou AZ, Klostermeier D. The DEAD-box helicase eIF4A: paradigm or the odd one out? RNA Biol. 2013;10(1):19–32.
18. Asthana S, Martin H, Rupkey J, Patel S, Yoon J, Keegan A et al. *„ The Physiological Roles of the Exon Junction Complex in Development and Diseases. Cells 2022, 11(7).*
19. Soderholm JF, Bird SL, Kalab P, Sampathkumar Y, Hasegawa K, Uehara-Bingen M, et al. Importazole, a small molecule inhibitor of the transport receptor importin-β. ACS Chem Biol. 2011;6(7):700–8.
20. Kumar V, Xin X, Ma J, Tan C, Osna N, Mahato RI. Therapeutic targets, novel drugs, and delivery systems for diabetes associated NAFLD and liver fibrosis. Adv Drug Deliv Rev. 2021;176:113888.
21. Maldonado MDM, Dharmawardhane S. Targeting Rac and Cdc42 GTPases in Cancer. Cancer Res. 2018;78(12):3101–11.

22. Chen J, Gu J, Tang M, Liao Z, Tang R, Zhou L, et al. Regulation of cancer progression by circRNA and functional proteins. J Cell Physiol. 2022;237(1):373–88.
23. Giorgi C, Yeo GW, Stone ME, Katz DB, Burge C, Turrigiano G, et al. The EJC factor eIF4AIII modulates synaptic strength and neuronal protein expression. Cell. 2007;130(1):179–91.
24. Jiang X, Guo S, Wang S, Zhang Y, Chen H, Wang Y, et al. EIF4A3-Induced circARHGAP29 promotes aerobic glycolysis in Docetaxel-resistant prostate Cancer through IGF2BP2/c-Myc/LDHA signaling. Cancer Res. 2022;82(5):831–45.
25. Xing W, Zhou P-C, Zhang H-Y, Chen L-M, Zhou Y-M, Cui X-F, et al. Circular RNA circ_GLIS2 suppresses hepatocellular carcinoma growth and metastasis. Liver Int. 2022;42(3):682–95.
26. Feng Z-H, Zheng L, Yao T, Tao S-Y, Wei X-A, Zheng Z-Y, et al. EIF4A3-induced circular RNA PRKAR1B promotes osteosarcoma progression by mir-361-3p-mediated induction of FZD4 expression. Cell Death Dis. 2021;12(11):1025.
27. Wei W, Sun J, Zhang H, Xiao X, Huang C, Wang L, et al. Circ0008399 Interaction with WTAP Promotes Assembly and Activity of the m6A methyltransferase complex and promotes cisplatin resistance in bladder Cancer. Cancer Res. 2021;81(24):6142–56.
28. Wang G, Sun D, Li W, Xin Y. CircRNA_100290 promotes GC cell proliferation and invasion via the miR-29b-3p/ITGA11 axis and is regulated by EIF4A3. Cancer Cell Int. 2021;21(1):324.
29. Zhou Q, Fu Q, Shaya M, Kugeluke Y, Li S, Dilimulati Y. Knockdown of circ_0055412 promotes cisplatin sensitivity of glioma cells through modulation of CAPG and Wnt/β-catenin signaling pathway. CNS Neurosci Ther. 2022;28(6):884–96.
30. Lu C, Rong D, Hui B, He X, Jiang W, Xu Y, et al. CircETFA upregulates CCL5 by sponging miR-612 and recruiting EIF4A3 to promote hepatocellular carcinoma. Cell Death Discov. 2021;7(1):321.
31. Yu F, Zhang Y, Wang Z, Gong W, Zhang C. Hsa_circ_0030042 regulates abnormal autophagy and protects atherosclerotic plaque stability by targeting eIF4A3. *Theranostics* 2021, 11(11): 5404–5417.
32. Mao S, Zhang W, Yang F, Guo Y, Wang H, Wu Y, et al. Hsa_circ_0004296 inhibits metastasis of prostate cancer by interacting with EIF4A3 to prevent nuclear export of ETS1 mRNA. J Exp Clin Cancer Res. 2021;40(1):336.
33. Li L, Wang J-Y, Yang C-Q, Jiang W. Effect of RhoA on transforming growth factor β1-induced rat hepatic stellate cell migration. Liver Int. 2012;32(7):1093–102.
34. Muhanna N, Doron S, Wald O, Horani A, Eid A, Pappo O, et al. Activation of hepatic stellate cells after phagocytosis of lymphocytes: a novel pathway of fibrogenesis. Hepatology. 2008;48(3):963–77.
35. Salat-Canela C, Pérez P, Ayté J, Hidalgo E. Stress-induced cell depolarization through the MAP kinase-Cdc42 axis. Trends Cell Biol. 2023;33(2):124–37.
36. Sun H, Kamanova J, Lara-Tejero M, Galán JE. Salmonella stimulates pro-inflammatory signaling through p21-activated kinases bypassing innate immune receptors. Nat Microbiol. 2018;3(10):1122–30.
37. Murphy NP, Mott HR, Owen D. Progress in the therapeutic inhibition of Cdc42 signaling. Biochem Soc Trans. 2021;49(3):1443–56.
38. He AT, Liu J, Li F, Yang BB. Targeting circular RNAs as a therapeutic approach: current strategies and challenges. Signal Transduct Target Therapy. 2021;6(1):185.
39. Singh S, Narang AS, Mahato RI. Subcellular fate and off-target effects of siRNA, shRNA, and miRNA. Pharm Res. 2011;28(12):2996–3015.
40. Reischl D, Zimmer A. Drug delivery of siRNA therapeutics: potentials and limits of nanosystems. Nanomedicine: Nanatechnol Biology Med. 2009;5(1):8–20.
41. Kulkarni JA, Witzigmann D, Chen S, Cullis PR, van der Meel R. Lipid nanoparticle technology for clinical translation of siRNA therapeutics. Acc Chem Res. 2019;52(9):2435–44.
42. Wu N, Xu J, Du WW, Li X, Awan FM, Li F, et al. YAP circular RNA, circYap, attenuates Cardiac Fibrosis via binding with Tropomyosin-4 and Gamma-actin decreasing actin polymerization. Mol Therapy: J Am Soc Gene Therapy. 2021;29(3):1138–50.
43. Hajiyeva A, Mamedov C, Gasimov E, Rzayev F, Isayev O, Khalilov R, et al. Ultrastructural investigation of iron oxide nanoparticles accumulation in the liver of common carp (Cyprinus carpio Linnaeus, 1758). Aquat Toxicol. 2024;272:106961.
44. Huseynov E. Novel nanomaterials for Hepatobiliary diseases Treatment and Future perspectives. Adv Biology Earth Sci. 2024;9(Special Issue):81–91.

Publisher's note